

Asymptotic-Preserving Neural Networks for Multiscale Kinetic Equations

Shi Jin^{1,2,4}, Zheng Ma^{1,2,3,5}, and Keke Wu^{1,*}

¹ School of Mathematical Sciences, Shanghai Jiao Tong University, Shanghai, 200240, P. R. China.

² Institute of Natural Sciences, MOE-LSC, Shanghai Jiao Tong University, Shanghai, 200240, P. R. China.

³ Qing Yuan Research Institute, Shanghai Jiao Tong University, Shanghai, 200240, China.

⁴ Shanghai Artificial Intelligence Laboratory, Shanghai, China.

⁵ CMA-Shanghai, Shanghai Jiao Tong University, Shanghai, China

Abstract. In this paper, we present two novel Asymptotic-Preserving Neural Networks (APNNs) for tackling multiscale time-dependent kinetic problems, encompassing the linear transport equation and Bhatnagar-Gross-Krook (BGK) equation in all ranges of Knudsen number. Our primary objective is to devise accurate APNN approaches for resolving multiscale kinetic equations, which is also efficient in the small Knudsen number regime. The first APNN for linear transport equation is based on even-odd decomposition, which relaxes the stringent conservation prerequisites while concurrently introducing an auxiliary deep neural network. We conclude that enforcing the initial condition for the linear transport equation with inflow boundary conditions is crucial for this network. For the Boltzmann-BGK equation, the APNN incorporates the conservation of mass, momentum, and total energy into the APNN framework as well as exact boundary conditions. A notable finding of this study is that approximating the zeroth, first, and second moments—which govern the conservation of density, momentum, and energy for the Boltzmann-BGK equation, is simpler than the distribution itself. Another interesting phenomenon observed in the training process is that the convergence of density is swifter than that of momentum and energy. Finally, we investigate several benchmark problems to demonstrate the efficacy of our proposed APNN methods.

AMS subject classifications: 65N30, 35J66, 41A46, 68T07

Key words: Asymptotic-Preserving Neural Networks, even-odd decomposition, conservation laws, multiscale.

1 Introduction

In scientific modeling, kinetic equations describe the dynamics of density distribution of particles that collide between themselves, or interacting with a medium or exter-

*Corresponding author. *Email addresses:* wukekever@sjtu.edu.cn (K. Wu)

nal fields. These equations are defined in the phase space, thus suffer from curse-of-dimensionality. In addition, they typically involve multiple spatial and/or temporal scales, characterized by the Knudsen number, as well as high dimensional nonlocal operators, hence present significant computational challenges in numerical simulations. For a comprehensive overview, please refer to the literature sources [1–4] for a review.

Deep learning methods and deep neural networks (DNNs) have garnered immense attention within the scientific community, including the possibility of resolving partial differential equations (PDEs) [5–12]. To explore alternative machine learning approaches for solving partial differential equations, we refer to the exemplary review article [5]. The key motivation behind such methods is to parameterize the solutions or gradients of PDE problems using deep neural networks. These methods ultimately culminate in a minimization problem that is typically high-dimensional and nonconvex. Unlike classical numerical methods, deep learning methods are mesh-free and can solve PDEs in high dimension, complex domains and geometries. It is also advantageous to possess flexibility and ease of execution. Nonetheless, deep learning methods have several potential drawbacks, including lengthy training times, a lack of convergence, and reduced accuracy. The idea of operator learning, on the other hand, offers a method to resolve a class of PDEs by training the neural network just *once* [13–18]. It is important to note, however, that a number of issues regarding the convergence theory remain unclear.

In recent years, there has been extensive research conducted on multiscale kinetic equations and hyperbolic systems by employing deep neural networks. This research includes, but is not limited to the works cited in references [19–21, 23–27]. In the design of DNNS, the definition of loss functions is crucial. There are numerous choices available to build the loss when given a PDE. For instance, the variational formulation (DRM), the least-squares formulation (PINN, DGM), the weak formulation (WAN), etc. Due to the presence of small scales, the vanilla Physics-Informed Neural Networks (PINNs) can perform poorly for resolving multiscale kinetic equations where small scales present [21, 23]. A natural question is what kind of loss is “good”. One important feature is to preserve important physical properties, such as conservation, symmetry, parity, entropy conditions, and asymptotic limits, etc. In our previous work [21], we developed a DNN for multiscale kinetic transport equations (with possible uncertainties) by creating a loss that can capture the limiting macroscopic behavior, as the Knudsen number approaches zero, satisfying a property known as Asymptotic-Preserving (AP), an asymptotic property known to be important in designing efficient numerical methods for multiscale kinetic equations [3, 22], hence justifies the need to use Asymptotic-Preserving Neural Networks (APNNs). This APNN method is based on the micro-macro decomposition, and we demonstrated that the loss is AP with respect to the Knudsen number when it tends to zero. It is worth noting that not all kinetic equations undergo a micro-macro decomposition. Even when applicable, designing neural networks that automatically satisfy conservation properties for nonlinear kinetic equations presents a challenging task [32, 33]. Taking the example of the nonlinear BGK equation, neural network approximations of solutions based on micro-macro decom-

position need to adhere to the local conservation of mass, momentum, and energy for the collision operator. While this conservation can be incorporated as soft constraints in the loss function, as mentioned in our previous work, such an approach has proven to compromise precision [21]. Consequently, we introduced a mechanism for embedding a mass conservation constraint directly into the neural network [21]. However, achieving a neural network that simultaneously satisfies mass, momentum, and energy conservation for the nonlinear BGK equation remains a formidable challenge.

In this work, we propose a different APNN that provides a framework for more general kinetic equations, with a generic way to handle both conservation and asymptotic properties in the loss functions. We contemplate incorporating redundant constraints into the new AP loss function which deviates from conventional AP numerical schemes. This, however, may be not a requirement in classical AP numerical schemes. The main idea is to involve both the original equation for macroscopic quantities, as well as the dynamic equations of the moments—that satisfy the conservation properties—in the loss functions. Evolving both dynamics have been used earlier for multiscale kinetic equations that allow the preservations of important moments at ease [36,38,39]. When such an idea is built into the loss function of DNN, it helps to loosen the stringent prerequisites for conservation. For the time-dependent linear transport equation, the proposed APNN technique relies on an even-odd decomposition. The novel loss function exhibits uniform stability with respect to the small Knudsen number, whereby the neural network solution formerly converges uniformly to the macro solution in the zero Knudsen number limit. Furthermore, we propose an APNN for the *nonlinear* Boltzmann-BGK equation, constructing deep neural networks that automatically satisfy the conservation of mass, momentum, and energy, akin to APNN based on a micro-macro decomposition [32] as in [21] poses a formidable challenge. Building the dynamics of moments into the loss function greatly alleviates this challenge. Thus, we have advanced by developing an APNN methodology that unites the fundamental equation with the equation governing local conservation law for the nonlinear Boltzmann-BGK equation.

An outline of this paper is as follows. In Section 2, a detailed illustration of Asymptotic-Preserving Neural Networks for linear transport equation and Boltzmann-BGK equation and the construction of loss functions are given. Numerous numerical examples are presented in Section 3 to demonstrate the effectiveness of the APNNs, as well as the issue of preserving positivity for density distribution in DNN. While our numerical examples are one-dimensional in space, we do include multidimensional uncertain variables, in order to demonstrate the ability of the network for high-dimensional problems. The paper is concluded in Section 4.

2 Methodology

There are three primary components to the DNN framework. The initial component entails utilizing a neural network as an approximation to the solution. The second component involves evaluating the difference between the approximate and exact solutions, which is achieved through population and empirical loss/risk. Finally, the

third component is an optimization algorithm that aids in locating a local minimum.

To solve partial differential equations using deep neural networks, the typical procedure is generally analogous:

1. Modeling: define the loss/risk associated with a PDE;
2. Architecture: build a deep neural network (function class) for the trial function;
3. Optimization: minimize the loss over the parameter space.

In terms of proposed APNNs, the primary element entails formulating a loss function that embodies the AP property [21]. The following diagram in Fig. 1 illustrates the idea of APNNs.

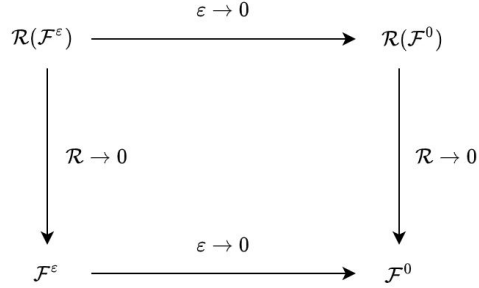


Figure 1: Illustration of APNNs. \mathcal{F}^ε is the microscopic equation that depends on the small scale parameter ε and \mathcal{F}^0 is its macroscopic limit as $\varepsilon \rightarrow 0$, which is independent of ε . The latent solution of \mathcal{F}^ε is approximated by deep neural networks with its measure denoted by $\mathcal{R}(\mathcal{F}^\varepsilon)$. The asymptotic limit of $\mathcal{R}(\mathcal{F}^\varepsilon)$ as $\varepsilon \rightarrow 0$, if exists, is denoted by $\mathcal{R}(\mathcal{F}^0)$. If $\mathcal{R}(\mathcal{F}^0)$ is a good measure of \mathcal{F}^0 , then it is called asymptotic-preserving (AP).

First, we introduce the conventional notations for DNNs[†]. An L -layer feed forward neural network (or fully-connected neural network, FCNet) is defined recursively as,

$$\begin{aligned}
 f_\theta^{[0]}(x) &= x, \\
 f_\theta^{[l]}(x) &= \sigma \circ (W^{[l-1]} f_\theta^{[l-1]}(x) + b^{[l-1]}), 1 \leq l \leq L-1, \\
 f_\theta(x) &= f_\theta^{[L]}(x) = W^{[L-1]} f_\theta^{[L-1]}(x) + b^{[L-1]},
 \end{aligned} \tag{2.1}$$

where $W^{[l]} \in \mathbb{R}^{m_{l+1} \times m_l}$, $b^{[l]} \in \mathbb{R}^{m_{l+1}}$, m_0, m_L are the input and output dimension, σ is a scalar function and “ \circ ” means entry-wise operation.

Also, ResNet [28] is composed with several residual blocks with each part containing one input, two weight layers, two activation functions, one identical (shortcut) con-

[†]BAAI.2020. Suggested Notation for Machine Learning. <https://github.com/mazhengcn/suggested-notation-for-machine-learning>.

nection, and one output, which is defined recursively as,

$$\begin{aligned} f_\theta^{[0]}(x) &= W^{[0]}x + b^{[0]}, \\ f_\theta^{[l]}(x) &= f_\theta^{[l-1]}(x) + \sigma \circ (W_2^{[l-1]} \sigma \circ (W_1^{[l-1]} f_\theta^{[l-1]}(x) + b_1^{[l-1]}) + b_2^{[l-1]}), 1 \leq l \leq L-1, \\ f_\theta(x) &= f_\theta^{[L]}(x) = W^{[L-1]} f_\theta^{[L-1]}(x) + b^{[L-1]}, \end{aligned} \quad (2.2)$$

here we use the same notations as previous for convenience.

We denote the set of parameters by θ . For simplicity of neural network presentation, we denote the layers by a list, i.e., $[m_0, \dots, m_L]$. For ResNet, the i -th block is denoted by $[m_i, m_i]$ and one can find that $m_i (i = 1, \dots, L-1)$ is equal.

2.1 APNN V2 based on even-odd decomposition

Let us begin by examining the linear transport equation in the context of diffusive scaling, which can be expressed in the following form:

$$\varepsilon \partial_t f + v \partial_x f = \frac{1}{\varepsilon} \left(\frac{1}{2} \int_{-1}^1 f \, dv' - f \right), \quad x_L < x < x_R, \quad -1 \leq v \leq 1, \quad (2.3)$$

with in-flow boundary conditions as

$$F_B = \begin{cases} f(t, x_L, v) = F_L(v), & \text{for } v > 0, \\ f(t, x_R, v) = F_R(v), & \text{for } v < 0. \end{cases} \quad (2.4)$$

Here, $f(t, x, v)$ is the density distribution of particles at time $t \in \mathcal{T}$, space point $x \in \mathcal{D}$, and traveling in direction $v \in \Omega := [-1, 1]$. The parameter $\varepsilon > 0$ is the Knudsen number which denotes the ratio of the mean free path over a characteristic length. The initial function is given as a function of x and v

$$f(0, x, v) = f_0(x, v). \quad (2.5)$$

By splitting equation and define even- and odd-parities as

$$\begin{aligned} r(t, x, v) &= \frac{1}{2} [f(t, x, v) + f(t, x, -v)], 0 \leq v \leq 1, \\ j(t, x, v) &= \frac{1}{2\varepsilon} [f(t, x, v) - f(t, x, -v)], 0 \leq v \leq 1, \end{aligned} \quad (2.6)$$

one can obtain the following system of equations

$$\begin{aligned} \partial_t r + v \partial_x j &= \frac{1}{\varepsilon^2} (\rho - r), \\ \partial_t j + \frac{1}{\varepsilon^2} v \partial_x r &= -\frac{1}{\varepsilon^2} j, \end{aligned} \quad (2.7)$$

where $\rho = \langle r \rangle := \int_0^1 r(t, x, v) \, dv$.

Thus far, we have implemented the even-odd system, which is the building-block of an AP scheme for the problem [29]. However, simply employing neural networks for r and j does not result in an APNN framework. In order to establish an APNN framework, our next step involves the introduction of ρ as a mediator between r and j within this system.

By integrating over v , the first equation gives

$$\partial_t \langle r \rangle + \int_0^1 v \partial_x j dv = \frac{1}{\varepsilon^2} (\rho - \langle r \rangle), \quad (2.8)$$

and since $\rho = \langle r \rangle$ one can write as follows

$$\partial_t \rho + \int_0^1 v \partial_x j dv = 0. \quad (2.9)$$

Finally, Eq. (2.7) and Eq. (2.9) together with the constraint $\rho = \langle r \rangle$ constitute the even-odd formulation of Eq. (2.3) to be used for our APNN:

$$\begin{cases} \varepsilon^2 \partial_t r + \varepsilon^2 v \partial_x j = \rho - r, \\ \varepsilon^2 \partial_t j + v \partial_x r = -j, \\ \partial_t \rho + \langle v \partial_x j \rangle = 0, \\ \rho = \langle r \rangle. \end{cases} \quad (2.10)$$

When $\varepsilon \rightarrow 0$, the above equation formally approaches

$$\begin{cases} r = \rho, \\ j = -v \partial_x r, \\ \partial_t \rho + \langle v \partial_x j \rangle = 0. \end{cases} \quad (2.11)$$

Substituting the first equation into the second equation gives $j = -v \partial_x \rho$ and plugging into the third equation will result

$$\partial_t \rho - \frac{1}{3} \partial_{xx} \rho = 0, \quad (2.12)$$

which is exactly the diffusion equation.

Remark 1. We emphasize that in Eq. (2.10), the equation of local conservation law– or the moment equation $\partial_t \rho + \langle v \partial_x j \rangle = 0$ is necessary in constructing the APNN loss in order to guarantee the AP property of the network. By coupling these equations of r, j and ρ , one can obtain the loss for the diffusion limit equation when $\varepsilon \rightarrow 0$. In [21], we exemplify the AP numerical scheme based on the even-odd method to illustrate that not all classical AP numerical formats are suitable for constructing APNN methods. The even-odd formulation for the linear transport equation is

$$\begin{aligned} \partial_t r + v \partial_x j &= \frac{1}{\varepsilon^2} (\langle r \rangle - r), \\ \partial_t j + \frac{1}{\varepsilon^2} v \partial_x r &= -\frac{1}{\varepsilon^2} j. \end{aligned} \quad (2.13)$$

It is noteworthy that within classical AP numerical schemes, the aforementioned Eq. (2.13) is already sufficiently solvable. However if one uses it in the loss, it will not be an APNN. To see this, consider the case when $\varepsilon \rightarrow 0$. Since the DNN will only pick up the leading term, one has, in the L^2 sense,

$$\begin{aligned} 0 &= \langle r \rangle - r, \\ j &= -v\partial_x r. \end{aligned} \quad (2.14)$$

These two equations will not lead to the diffusion equation. This is because the corresponding loss function mentioned above does not provide the evolution process of the macroscopic quantity $\rho = \langle r \rangle$. This omission results in the neural network's approximated solution stagnating at the initial conditions.

For solving the linear transport equation by deep neural networks, we need to use DNNs to parametrize three functions $\rho(t, x)$, $r(t, x, v)$ and $j(t, x, v)$. So here three networks are used. First,

$$\rho_\theta^{\text{NN}}(t, x) := \exp\left(-\tilde{\rho}_\theta^{\text{NN}}(t, x)\right) \approx \rho(t, x), \quad (2.15)$$

Second,

$$r_\theta^{\text{NN}}(t, x, v) := \exp\left(-\frac{1}{2}(\tilde{r}_\theta^{\text{NN}}(t, x, v) + \tilde{r}_\theta^{\text{NN}}(t, x, -v))\right) \approx r(t, x, v), \quad (2.16)$$

and

$$j_\theta^{\text{NN}}(t, x, v) := \tilde{j}_\theta^{\text{NN}}(t, x, v) - \tilde{j}_\theta^{\text{NN}}(t, x, -v) \approx j(t, x, v), \quad (2.17)$$

which automatically satisfy the even-odd properties.

Then we propose the least square of the residual of the even-odd system as the APNN loss

$$\mathcal{R}_{\text{APNN}}^\varepsilon = \mathcal{R}_{\text{residual}}^\varepsilon + \mathcal{R}_{\text{constraint}}^\varepsilon + \mathcal{R}_{\text{initial}}^\varepsilon + \mathcal{R}_{\text{boundary}}^\varepsilon, \quad (2.18)$$

where $\mathcal{R}_{\text{residual}}^\varepsilon, \mathcal{R}_{\text{constraint}}^\varepsilon, \mathcal{R}_{\text{initial}}^\varepsilon, \mathcal{R}_{\text{boundary}}^\varepsilon$ are denoted by

$$\begin{aligned} \mathcal{R}_{\text{residual}}^\varepsilon &= \frac{\lambda_1}{|\mathcal{T} \times \mathcal{D} \times \Omega|} \int_{\mathcal{T}} \int_{\mathcal{D}} \int_{\Omega} |\varepsilon^2 \partial_t r_\theta^{\text{NN}} + \varepsilon^2 v \partial_x j_\theta^{\text{NN}} - (\rho_\theta^{\text{NN}} - r_\theta^{\text{NN}})|^2 dv dx dt \\ &\quad + \frac{\lambda_2}{|\mathcal{T} \times \mathcal{D} \times \Omega|} \int_{\mathcal{T}} \int_{\mathcal{D}} \int_{\Omega} |\varepsilon^2 \partial_t j_\theta^{\text{NN}} + v \partial_x r_\theta^{\text{NN}} - (-j_\theta^{\text{NN}})|^2 dv dx dt \\ &\quad + \frac{\lambda_3}{|\mathcal{T} \times \mathcal{D}|} \int_{\mathcal{T}} \int_{\mathcal{D}} |\partial_t \rho_\theta^{\text{NN}} + \langle v \partial_x j_\theta^{\text{NN}} \rangle|^2 dx dt, \\ \mathcal{R}_{\text{constraint}}^\varepsilon &= \frac{\lambda_4}{|\mathcal{T} \times \mathcal{D}|} \int_{\mathcal{T}} \int_{\mathcal{D}} |\rho_\theta^{\text{NN}} - \langle r_\theta^{\text{NN}} \rangle|^2 dx dt, \\ \mathcal{R}_{\text{initial}}^\varepsilon &= \frac{\lambda_5}{|\mathcal{D}|} \int_{\mathcal{D}} |\rho_\theta^{\text{NN}}(0, x) - \langle f_0 \rangle|^2 dx + \frac{\lambda_6}{|\mathcal{D} \times \Omega|} \int_{\mathcal{D}} \int_{\Omega} |\mathcal{I}(r_\theta^{\text{NN}} + \varepsilon j_\theta^{\text{NN}}) - f_0|^2 dv dx, \\ \mathcal{R}_{\text{boundary}}^\varepsilon &= \frac{\lambda_7}{|\mathcal{T} \times \partial \mathcal{D} \times \Omega|} \int_{\mathcal{T}} \int_{\partial \mathcal{D}} \int_{\Omega} |\mathcal{B}(r_\theta^{\text{NN}} + \varepsilon j_\theta^{\text{NN}}) - F_B|^2 dv dx dt. \end{aligned} \quad (2.19)$$

Here, λ_i ($i = 1, 2, \dots, 7$) are the penalty weights to be tuned and $\mathcal{T}, \mathcal{D}, \Omega$ represent the bounded domains of time, space and velocity space, respectively. $|\mathcal{X}|$ denotes the measure of the domain \mathcal{X} . Besides, \mathcal{I}, \mathcal{B} are the initial and boundary operators.

Now the AP property of this loss can be carried out by considering its behavior for ε small. One may only need to focus on the first three terms of Eq. (2.19)

$$\begin{aligned} \mathcal{R}_{\text{residual}}^\varepsilon &= \frac{\lambda_1}{|\mathcal{T} \times \mathcal{D} \times \Omega|} \int_{\mathcal{T}} \int_{\mathcal{D}} \int_{\Omega} |\varepsilon^2 \partial_t r_\theta^{\text{NN}} + \varepsilon^2 v \partial_x j_\theta^{\text{NN}} - (\rho_\theta^{\text{NN}} - r_\theta^{\text{NN}})|^2 dv dx dt \\ &\quad + \frac{\lambda_2}{|\mathcal{T} \times \mathcal{D} \times \Omega|} \int_{\mathcal{T}} \int_{\mathcal{D}} \int_{\Omega} |\varepsilon^2 \partial_t j_\theta^{\text{NN}} + v \partial_x r_\theta^{\text{NN}} - (-j_\theta^{\text{NN}})|^2 dv dx dt \\ &\quad + \frac{\lambda_3}{|\mathcal{T} \times \mathcal{D}|} \int_{\mathcal{T}} \int_{\mathcal{D}} |\partial_t \rho_\theta^{\text{NN}} + \langle v \partial_x j_\theta^{\text{NN}} \rangle|^2 dx dt. \end{aligned} \quad (2.20)$$

Sending $\varepsilon \rightarrow 0$, this will naturally lead to

$$\begin{aligned} \mathcal{R}_{\text{residual}}^0 &= \frac{\lambda_1}{|\mathcal{T} \times \mathcal{D} \times \Omega|} \int_{\mathcal{T}} \int_{\mathcal{D}} \int_{\Omega} |\rho_\theta^{\text{NN}} - r_\theta^{\text{NN}}|^2 dv dx dt \\ &\quad + \frac{\lambda_2}{|\mathcal{T} \times \mathcal{D} \times \Omega|} \int_{\mathcal{T}} \int_{\mathcal{D}} \int_{\Omega} |v \partial_x r_\theta^{\text{NN}} - (-j_\theta^{\text{NN}})|^2 dv dx dt \\ &\quad + \frac{\lambda_3}{|\mathcal{T} \times \mathcal{D}|} \int_{\mathcal{T}} \int_{\mathcal{D}} |\partial_t \rho_\theta^{\text{NN}} + \langle v \partial_x j_\theta^{\text{NN}} \rangle|^2 dx dt, \end{aligned} \quad (2.21)$$

which is the least square loss of Eq. (2.11)

$$\begin{cases} r = \rho, \\ j = -v \partial_x r, \\ \partial_t \rho + \langle v \partial_x j \rangle = 0. \end{cases} \quad (2.22)$$

Same as previous derivation the third equation yields the diffusion Eq. (2.12). Thus this proposed method is an APNN method.

Remark 2. Additionally, one can try two Deep Neural Networks, namely r_θ and j_θ , to approximate r and j without ρ with the AP loss described by the following equations:

$$\begin{aligned} \partial_t r + v \partial_x j &= \frac{1}{\varepsilon^2} (\langle r \rangle - r), \\ \partial_t j + \frac{1}{\varepsilon^2} v \partial_x r &= -\frac{1}{\varepsilon^2} j, \\ \partial_t \langle r \rangle + \langle v \partial_x j \rangle &= 0. \end{aligned} \quad (2.23)$$

In our article, we use extra DNNs to approximate macroscopic quantities inspired by the relaxation schemes [34].

2.2 APNN for the Boltzmann-BGK equation

The Boltzmann equation is the well-known kinetic model which captures the evolution of density distribution for rarefied gases [30,31]. The one-dimensional Boltzmann equation can be expressed in a dimensionless form as

$$\partial_t f + v \cdot \nabla_x f = \frac{1}{\varepsilon} \mathcal{C}(f, f), \quad t > 0, \quad (x, v) \in \mathbb{R} \times \mathbb{R}, \quad (2.24)$$

where the function, denoted by $f(t, x, v)$, is the density distribution of particles, while the right-hand side of the equation $\frac{1}{\varepsilon} \mathcal{C}(f, f)$ represents the term associated with binary collisions between particles and is a non-linear operator. Its action is generally limited to the velocity-dependent behavior of f exclusively. The parameter $\varepsilon > 0$ is the Knudsen number which denotes the ratio of the mean free path over a characteristic length.

The so-called Boltzmann collision operator $\mathcal{C}(f, f)$ possesses fundamental physical properties [32] as

1. conservation of mass, momentum and energy

$$\int_{\mathbb{R}} m \mathcal{C}(f, f) dv = 0, \quad m = \left(1, v, \frac{1}{2}|v|^2\right)^T.$$

2. The entropy dissipation inequality (the H-Theorem)

$$\int_{\mathbb{R}} \mathcal{C}(f, f) \cdot \log(f) dv \leq 0.$$

3. The non-negative equilibrium functions f , namely those satisfying $\mathcal{C}(f, f) = 0$, correspond to the local Maxwellian distributions defined by

$$M(U) = \frac{\rho}{(2\pi T)^{\frac{1}{2}}} \exp\left(-\frac{|v-u|^2}{2T}\right), \quad (2.25)$$

where density $\rho(t, x)$, macroscopic velocity $u(t, x)$ and temperature $T(t, x)$ of the gas are the continuum description by field variables defined by

$$\begin{aligned} \rho &= \int_{\mathbb{R}} f(v) dv = \int_{\mathbb{R}} M(U) dv, \\ u &= \frac{1}{\rho} \int_{\mathbb{R}} v f(v) dv = \frac{1}{\rho} \int_{\mathbb{R}} v M(U) dv, \\ T &= \frac{1}{\rho} \int_{\mathbb{R}} |u-v|^2 f(v) dv = \frac{1}{\rho} \int_{\mathbb{R}} |u-v|^2 M(U) dv. \end{aligned}$$

Here, U is the hydrodynamic variables (density, momentum and energy) which is a vector of the moments of f :

$$U = \left(\rho, \rho u, \frac{1}{2}\rho|u|^2 + \frac{1}{2}\rho T\right)^T = \int_{\mathbb{R}} m f dv, \quad (2.26)$$

and density $\rho(t, x)$, macroscopic velocity $u(t, x)$ and temperature $T(t, x)$ are macroscopic quantities.

As the frequency of collisions increases significantly, the mean free path, i.e., the distance a particle travels between two consecutive collisions, becomes comparatively smaller than the characteristic length of the physical domain under consideration. In such a scenario, a macroscopic portrayal of the gas seems more suitable. The compressible Euler and compressible Navier-Stokes (CNS) equations serve as primary instances, as they elucidate the dynamics of macroscopic quantities like the local density, momentum, and energy of the gas. The CNS model surpasses the Euler equations in terms of accuracy, owing to its inclusion of factors such as viscosity and heat conductivity, which results in a correction of order ε . Physically, classical fluid models may not fully capture the macroscopic evolution of gas, particularly when it is far away from the equilibrium state when the Knudsen number is large.

Fluid models, such as the compressible Euler or CNS type, are classically derived by using the moment method in conjunction with perturbation techniques like the Hilbert or Chapman-Enskog expansions [31]. Specifically, the derivation of the CNS model from the Boltzmann equation in the fluid regime provides an approximation of viscosity and heat fluxes in the gas, up to the order of ε^2 . The primary challenge of solving the Boltzmann equation stems from the fact that the aforementioned term $\frac{1}{\varepsilon}$ stiffens as ε approaches zero, thereby entering a fluid regime. When considering this scenario, the resolution of the Boltzmann equation through a conventional explicit numerical method necessitates a time step of ε magnitude. This results in computationally costly operations when ε is small. At the level of Euler asymptotics, numerous authors have suggested asymptotically preserving numerical approximations to solve the Boltzmann equation. For instance, numerical methods that are capable of capturing the accurate Euler limit have been proposed in [32, 35, 36].

The intricate nature of the Boltzmann collision operator is circumvented by considering the simpler BGK model [37] in our study as follows

$$\partial_t f + v \cdot \nabla_x f = \frac{1}{\varepsilon} (M(U) - f), \quad v \in \mathbb{R}, \quad (2.27)$$

here $f(t, x, v)$ is the density distribution of particles at time $t \in \mathcal{T}$, space point $x \in \mathcal{D}$, and traveling in direction $v \in \mathbb{R}$, $M(U)$ denotes the local Maxwellian distribution function. Notice that the Boltzmann-BGK equation is an integro-differential equation with its nonlinear and non-local collision operator. One can easily check that BGK operator satisfies mass, momentum and energy conservation.

Due to the properties of conserving mass, momentum and energy of collision operator, one can multiply the BGK equation Eq. (2.27) by $m(v)$ and then integrate them with respect to v to obtain the following equations:

$$\partial_t \langle mf \rangle + \nabla_x \cdot \langle vmf \rangle = 0, \text{ where } \langle g \rangle = \int_{\mathbb{R}} g(v) dv, \quad (2.28)$$

i.e.,

$$\partial_t \begin{pmatrix} \rho \\ \rho u \\ \frac{1}{2}\rho|u|^2 + \frac{1}{2}\rho T \end{pmatrix} + \nabla_x \cdot \langle vmf \rangle = 0. \quad (2.29)$$

The equivalent formulation of Eq. (2.29) is

$$\partial_t \begin{pmatrix} \rho \\ \rho u \\ E \end{pmatrix} + \nabla_x \cdot \begin{pmatrix} \rho u \\ \rho u^2 + P \\ Eu + Pu + Q \end{pmatrix} = 0, \quad (2.30)$$

where $E = \frac{1}{2}\rho u^2 + \frac{1}{2}\rho T$ is the energy, $P = \int_{\mathbb{R}} |u-v|^2 f(v) dv$ denotes the pressure tensor, and $Q = \int_{\mathbb{R}} (v-u)|u-v|^2 f(v) dv$ represents the heat flux. When taking the limit as ε approaches zero, the density function f will converge towards a local Maxwellian distribution $M(U)$. Under this approximation, the pressure tensor P and the heat flux Q can be expressed as $P = pI$ and $Q = 0$, respectively, where $p = \rho T$ represents the pressure and I denotes the identity matrix. Eq. (2.30) reduces to the compressible Euler equations

$$\partial_t \begin{pmatrix} \rho \\ \rho u \\ E \end{pmatrix} + \nabla_x \cdot \begin{pmatrix} \rho u \\ \rho u^2 + pI \\ (E+p)u \end{pmatrix} = 0. \quad (2.31)$$

Finally, Eq. (2.27) and Eq. (2.29) with the constraint Eq. (2.26) constitute the systems of BGK model for our APNN:

$$\begin{cases} \varepsilon(\partial_t f + v\partial_x f) = M(U) - f, \\ \partial_t U + \nabla_x \cdot \langle vmf \rangle = 0, \\ U = \langle mf \rangle. \end{cases} \quad (2.32)$$

The aforementioned idea was initially introduced in [38], wherein the employment of asymptotic-preserving schemes was demonstrated for the Fokker-Planck-Landau equation. Subsequently, it was further explored in [39], focusing on the development of asymptotic-preserving numerical schemes and the conservation of numerical moments for collisional nonlinear kinetic equations. While considering the Boltzmann-BGK equation, similar to APNN in [21], it is crucial to highlight that our observation indicates the difficulty in creating a neural network for the non-equilibrium that adequately maintains the simultaneous conservation of mass, momentum and energy, despite its micro-macro decomposition technique for resolution [32]. Thus, inspired by the idea of evolving both density distribution and moments for conservation properties [38,39], we incorporated the original equation concerning function f into the system of local conservation laws Eq. (2.28) or Eq. (2.29), thereby closing the newly established system of equations.

First we need to use DNNs to parametrize four functions $f(t,x,v), \rho(t,x), u(t,x)$ and $T(t,x)$. So here four networks are used: $\rho_\theta(t,x), u_\theta(t,x), T_\theta(t,x), f_\theta(t,x,v)$. Besides, we restrict the range of velocity \mathbb{R} to a bounded symmetrical domain $\Omega = [-V, V]$ and this assumption is used in most computations of the model. The time and velocity

variable t, v are normalized into $[0, 1]$ and $[-1, 1]$ with scaling $\bar{t} = t/T, \bar{v} = v/V$. It is worth pointing out that this normalization is necessary to alleviate the mismatching of the range of temporal domain and velocity domain. For brevity we use the notation $W(t, x) = (\rho(t, x), u(t, x), T(t, x))^T$ and $W_\theta^{\text{NN}}(t, x) = (\rho_\theta^{\text{NN}}(t, x), u_\theta^{\text{NN}}(t, x), T_\theta^{\text{NN}}(t, x))^T$.

Then we propose the least square of the residual of BGK model as the APNN loss

$$\mathcal{R}_{\text{APNN}}^\varepsilon = \mathcal{R}_{\text{residual}}^\varepsilon + \mathcal{R}_{\text{claw}}^\varepsilon + \mathcal{R}_{\text{constraint}}^\varepsilon + \mathcal{R}_{\text{boundary}}^\varepsilon + \mathcal{R}_{\text{initial}}^\varepsilon, \quad (2.33)$$

where $\mathcal{R}_{\text{residual}}^\varepsilon, \mathcal{R}_{\text{claw}}^\varepsilon, \mathcal{R}_{\text{constraint}}^\varepsilon, \mathcal{R}_{\text{boundary}}^\varepsilon, \mathcal{R}_{\text{initial}}^\varepsilon$ are denoted by

$$\begin{aligned} \mathcal{R}_{\text{residual}}^\varepsilon &= \frac{\lambda_1}{|\mathcal{T} \times \mathcal{D} \times \Omega|} \int_{\mathcal{T}} \int_{\mathcal{D}} \int_{\Omega} |\varepsilon(\partial_t f_\theta^{\text{NN}} + v \nabla_x f_\theta^{\text{NN}}) - (M(U_\theta^{\text{NN}}) - f_\theta^{\text{NN}})|^2 dv dx dt, \\ \mathcal{R}_{\text{claw}}^\varepsilon &= \frac{\lambda_2}{|\mathcal{T} \times \mathcal{D}|} \int_{\mathcal{T}} \int_{\mathcal{D}} |\partial_t U_\theta^{\text{NN}} + \nabla_x \langle v m f_\theta^{\text{NN}} \rangle|^2 dx dt, \\ \mathcal{R}_{\text{constraint}}^\varepsilon &= \frac{\lambda_3}{|\mathcal{T} \times \mathcal{D}|} \int_{\mathcal{T}} \int_{\mathcal{D}} |U_\theta^{\text{NN}} - \langle m f_\theta^{\text{NN}} \rangle|^2 dx dt, \\ \mathcal{R}_{\text{boundary}}^\varepsilon &= \frac{\lambda_4}{|\mathcal{T} \times \partial \mathcal{D}|} \int_{\mathcal{T} \times \partial \mathcal{D}} |W_\theta^{\text{NN}}(t, x) - W(t, x)|^2 dx dt, \\ \mathcal{R}_{\text{initial}}^\varepsilon &= \frac{\lambda_5}{|\mathcal{D}|} \int_{\mathcal{D}} |W_\theta^{\text{NN}}(0, x) - W(0, x)|^2 dx + \frac{\lambda_6}{|\mathcal{D} \times \Omega|} \int_{\mathcal{D}} \int_{\Omega} |f_\theta^{\text{NN}}(0, x, v) - f(0, x, v)|^2 dv dx, \end{aligned} \quad (2.34)$$

and $U_\theta^{\text{NN}}, W_\theta^{\text{NN}}$ are computed by $\rho_\theta^{\text{NN}}, u_\theta^{\text{NN}}$ and T_θ^{NN} .

The AP property of this loss can now be realized by examining its behavior for infinitesimally small values of ε . One may only need to focus on the first two terms of Eq. (2.33)

$$\mathcal{R}_{\text{APNN}}^\varepsilon = \mathcal{R}_{\text{residual}}^\varepsilon + \mathcal{R}_{\text{claw}}^\varepsilon, \quad (2.35)$$

$$\begin{aligned} \mathcal{R}_{\text{residual}}^\varepsilon &= \frac{\lambda_1}{|\mathcal{T} \times \mathcal{D} \times \Omega|} \int_{\mathcal{T}} \int_{\mathcal{D}} \int_{\Omega} |\varepsilon(\partial_t f_\theta^{\text{NN}} + v \nabla_x f_\theta^{\text{NN}}) - (M(U_\theta^{\text{NN}}) - f_\theta^{\text{NN}})|^2 dv dx dt, \\ \mathcal{R}_{\text{claw}}^\varepsilon &= \frac{\lambda_2}{|\mathcal{T} \times \mathcal{D}|} \int_{\mathcal{T}} \int_{\mathcal{D}} |\partial_t U_\theta^{\text{NN}} + \nabla_x \langle v m f_\theta^{\text{NN}} \rangle|^2 dx dt. \end{aligned} \quad (2.36)$$

Sending $\varepsilon \rightarrow 0$, this will naturally lead to

$$\begin{aligned} \mathcal{R}_{\text{residual}}^0 &= \frac{\lambda_1}{|\mathcal{T} \times \mathcal{D} \times \Omega|} \int_{\mathcal{T}} \int_{\mathcal{D}} \int_{\Omega} |M(U_\theta^{\text{NN}}) - f_\theta^{\text{NN}}|^2 dv dx dt, \\ \mathcal{R}_{\text{claw}}^0 &= \frac{\lambda_2}{|\mathcal{T} \times \mathcal{D}|} \int_{\mathcal{T}} \int_{\mathcal{D}} |\partial_t U_\theta^{\text{NN}} + \nabla_x \langle v m f_\theta^{\text{NN}} \rangle|^2 dx dt, \end{aligned} \quad (2.37)$$

which is the least square loss of fluid dynamics equations, i.e., Eq. (2.31).

Thus, we have check that this loss is AP by sending $\varepsilon \rightarrow 0$. Finally we put a schematic plot of our APNN method for Boltzmann-BGK problem in Fig. 2.

3 Numerical results

In this section, some numerical experiments will be carried out to verify the performance of our proposed APNN methods. Since the operator of v in the loss of APNNs are integrals, we approximate them with the Gauss-Legendre quadrature rule.

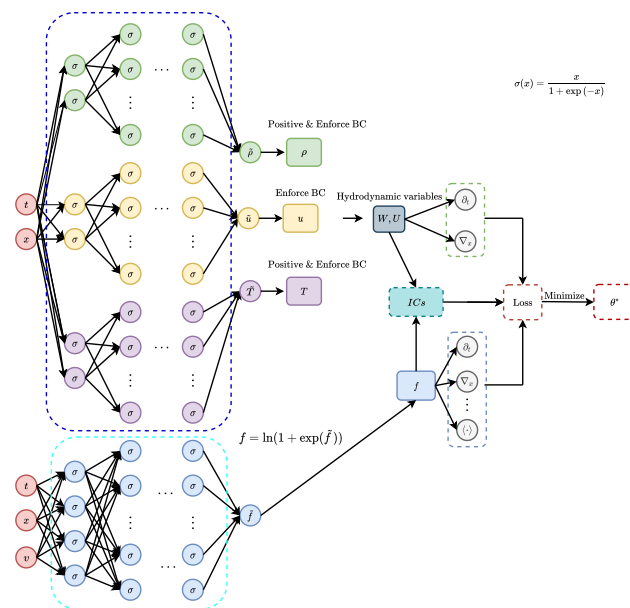


Figure 2: Schematic of APNNs for solving the Boltzmann-BGK equation.

The reference solutions are obtained by standard finite difference method and we will check the relative ℓ^2 error of the solution $s(x)(\rho, u, T)$ of the APNN method, e.g. for 1d case,

$$\text{error} := \sqrt{\frac{\sum_j |s_{\theta,j}^{\text{NN}} - s_j^{\text{ref}}|^2}{\sum_j |s_j^{\text{ref}}|^2}}. \quad (3.1)$$

3.1 Experiment setting

The activation function we used is $\sigma(x) = \tanh(x)$ for linear transport problems and $\sigma(x) = x/(1 + \exp(-x))$ for BGK problems. More specifically, fully-connected neural network is applied to the linear transport problem while ResNet is used for the BGK problem for better performance. In particular, the spatial domain of interest, denoted as \mathcal{D} , includes the interval $[0,1]$ for the linear transport equation and $[-0.5,0.5]$ for the Boltzmann-BGK equation. Additionally, the parameter V is assigned a value of 10. The number of quadrature points is 30 for the linear transport equation and 64 for the Boltzmann-BGK equation. To train the networks, the Adam [42] version of the gradient

descent methods is used to solve the optimization problem with Xavier initialization. In practice of these cases, we need to tune the hyperparameters, such as neural network architecture, learning rate, batch size and so on, to obtain a good level of accuracy [43]. As a matter of experience one may tune the weights of loss terms to make them at the same level and a decreasing annealing schedule for learning rate is used for better numerical performance. We use an exponential decay strategy for an initial learning rate $\eta_0 = 10^{-3}$ with a decay rate of $\gamma = 0.96$ and a decay step of $p = 200$ iterations:

$$\eta_i = \eta_0 \cdot \gamma^{\lfloor \frac{i}{p} \rfloor},$$

here, the variable i represents the current i -th iteration step, and the symbol $\lfloor \cdot \rfloor$ denotes the floor function.

3.2 Problem 1: APNNs for solving linear transport equations

Consider the linear transport equation:

$$\varepsilon \partial_t f + v \partial_x f = \frac{1}{\varepsilon} \left(\frac{1}{2} \int_{-1}^1 f \, dv' - f \right),$$

and recall that the even-odd system of the equation is

$$\begin{cases} \varepsilon^2 \partial_t r + \varepsilon^2 v \partial_x j = \rho - r, \\ \varepsilon^2 \partial_t j + v \partial_x r = -j, \\ \partial_t \rho + \langle v \partial_x j \rangle = 0, \\ \rho = \langle r \rangle. \end{cases}$$

The APNN empirical risk for the even-odd system of linear transport equation is

$$\mathcal{R}_{\text{APNN, transport}}^\varepsilon = \mathcal{R}_{\text{residual}}^\varepsilon + \mathcal{R}_{\text{constraint}}^\varepsilon + \mathcal{R}_{\text{initial}}^\varepsilon + \mathcal{R}_{\text{boundary}}^\varepsilon, \quad (3.2)$$

where $\mathcal{R}_{\text{residual}}^\varepsilon, \mathcal{R}_{\text{constraint}}^\varepsilon, \mathcal{R}_{\text{initial}}^\varepsilon, \mathcal{R}_{\text{boundary}}^\varepsilon$ are denoted by

$$\begin{aligned}
\mathcal{R}_{\text{residual}}^\varepsilon &= \frac{\lambda_1}{N_1^{(1)}} \sum_{i=1}^{N_1^{(1)}} |\varepsilon^2 \partial_t r_\theta^{\text{NN}}(t_i, x_i, v_i) + \varepsilon^2 v \partial_x j_\theta^{\text{NN}}(t_i, x_i, v_i) \\
&\quad - (\rho_\theta^{\text{NN}}(t_i, x_i) - r_\theta^{\text{NN}}(t_i, x_i, v_i))|^2 \\
&\quad + \frac{\lambda_2}{N_1^{(2)}} \sum_{i=1}^{N_1^{(2)}} |\varepsilon^2 \partial_t j_\theta^{\text{NN}}(t_i, x_i, v_i) + v \partial_x r_\theta^{\text{NN}}(t_i, x_i, v_i) - (-j_\theta^{\text{NN}}(t_i, x_i, v_i))|^2 \\
&\quad + \frac{\lambda_3}{N_1^{(3)}} \sum_{i=1}^{N_1^{(3)}} |\partial_t \rho_\theta^{\text{NN}}(t_i, x_i) + \langle v \partial_x j_\theta^{\text{NN}} \rangle(t_i, x_i)|^2, \\
\mathcal{R}_{\text{constraint}}^\varepsilon &= \frac{\lambda_4}{N_2} \sum_{i=1}^{N_2} |\rho_\theta^{\text{NN}}(t_i, x_i) - \langle r_\theta^{\text{NN}} \rangle(t_i, x_i)|^2, \\
\mathcal{R}_{\text{initial}}^\varepsilon &= \frac{\lambda_5}{N_3} \sum_{i=1}^{N_3} |\rho_\theta^{\text{NN}}(0, x_i) - \langle f_0 \rangle(x_i)|^2 + \frac{\lambda_6}{N_4} \sum_{i=1}^{N_4} |\mathcal{I}(r_\theta^{\text{NN}} + \varepsilon j_\theta^{\text{NN}})(x_i, v_i) - f_0(x_i, v_i)|^2, \\
\mathcal{R}_{\text{boundary}}^\varepsilon &= \frac{\lambda_7}{N_5} \sum_{i=1}^{N_5} |\mathcal{B}(r_\theta^{\text{NN}} + \varepsilon j_\theta^{\text{NN}})(t_i, x_i, v_i) - F_B(t_i, x_i, v_i)|^2.
\end{aligned} \tag{3.3}$$

Here, $N_1^{(1)}, N_1^{(2)}, N_1^{(3)}, N_2, N_3, N_4, N_5$ are the number of uniform sampling points of domains $|\mathcal{T} \times \mathcal{D} \times \Omega|, |\mathcal{T} \times \mathcal{D} \times \Omega|, |\mathcal{T} \times \mathcal{D}|, |\mathcal{T} \times \mathcal{D}|, |\mathcal{D}|, |\mathcal{D} \times \Omega|, |\mathcal{T} \times \partial \mathcal{D} \times \Omega|$.

Case I and II are studied for problem 1 with constant scattering coefficient 1 for $\varepsilon = 10^{-3}, 10^{-8}$. Furthermore, we focus on an uncertainty quantification problem for $\varepsilon = 10^{-5}$ in Case III.

Case I. Inflow condition with $\varepsilon = 10^{-3}$

Consider $\varepsilon = 10^{-3}$, and the inflow boundary conditions are defined as $F_L(v) = 1$ and $F_R(v) = 0$, indicating the specified values of the distribution function at the left and right boundaries, respectively. The initial condition is set as $f_0(x, v) = 0$, denoting the initial distribution function. Note that the function f exhibits a discontinuity at $t = 0$ due to the conditions $F_L(v) = 1, F_R(v) = 0$, and $f_0(x, v) = 0$. To enhance numerical performance, ρ_θ^{NN} can be further designed to inherently satisfy the initial condition.:

$$\rho_\theta^{\text{NN}}(t, x) := t \cdot \exp\left(-\tilde{\rho}_\theta^{\text{NN}}(t, x)\right) \approx \rho(t, x). \tag{3.4}$$

Fig. 3 depicts the estimated density, denoted as ρ , using APNNs in comparison to the reference solution at time instances $t=0, 0.05, 0.1$. It is evident that the approximated solutions exhibit favorable accuracy at both $t=0, 0.05$ and $t=0.1$.

The numerical performance of enforcing the initial condition and the soft constraint $\rho = \langle r \rangle$ is deliberated as follows. The ensuing phenomena have been observed in all the experiments we have conducted.

Fig. 4 illustrates the performance resulting from the improper enforcement of the initial condition. Owing to the inadequate approximation of the initial condition and

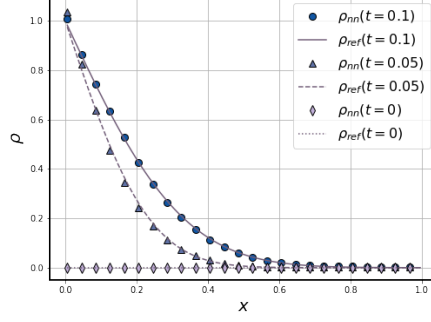


Figure 3: Problem 1—Case I. Plot of density ρ at $t=0,0.05,0.1$: APNNs (marker) vs. Ref (line). $\varepsilon=10^{-3}$ and neural networks are FCNet with units $[2,128,128,128,128,1]$ for ρ and $[3,256,256,256,256,1]$ both for r and j . Batch size is 512 in domain, 1024×2 on boundary and 512 on initial condition. $\lambda_7=10$ and other λ 's are set to be 1. Relative ℓ^2 error of APNNs is 9.87×10^{-3} .

the influence of the boundary layer, erroneous solutions are obtained at time instances $t=0,0.05,0.1$.

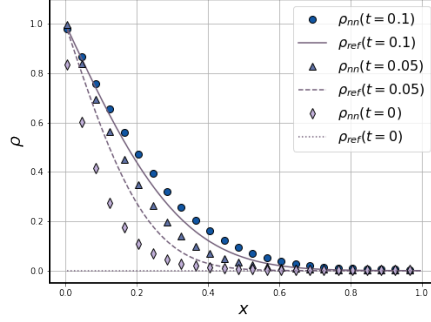


Figure 4: Problem 1—Case I. Plot of density ρ at $t=0,0.05,0.1$: APNNs (marker) vs. Ref (line). $\varepsilon=10^{-3}$. And the units of neural networks are $[2,128,128,128,128,1]$ for ρ and $[3,256,256,256,256,1]$ both for r and j .

Fig. 5 illustrates the performance in the absence of the constraint equation $\rho = \langle r \rangle$ in the loss function, while ensuring the exact satisfaction of the initial condition. However, it is evident that the solutions at time $t=0.05,0.1$ are incorrect. Consequently, we incorporate this constraint into our APNN loss function.

Case II. The homogeneous Dirichlet boundary condition with $\varepsilon=10^{-8}$

Let $\varepsilon=10^{-8}$, boundary condition be $F_L(v) = F_R(v) = 0$, and initial condition be

$$f_0(x,v) = g(x) \cdot \frac{3}{\sqrt{2\pi}} e^{-\frac{(3v)^2}{2}}, \quad (3.5)$$

where

$$g(x) = 1 + \sin\left(2\pi x - \frac{\pi}{2}\right). \quad (3.6)$$

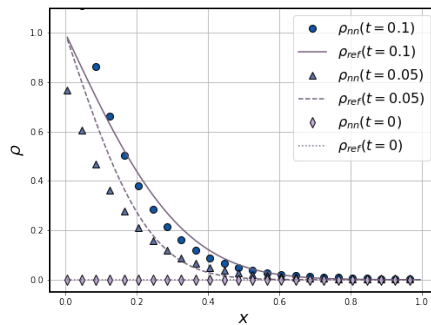


Figure 5: Problem 1—Case I. Plot of density ρ at $t=0,0.05,0.1$: APNNs (marker) vs. Ref (line). $\varepsilon=10^{-3}$. And the units of neural networks are $[2,128,128,128,128,1]$ for ρ and $[3,256,256,256,256,1]$ both for r and j .

Fig. 6 depicts the estimated density, denoted as ρ , obtained through the utilization of APNNs alongside the reference solution at three distinct time instances, namely $t=0,0.05,0.1$. In this particular scenario, it is noteworthy that the function f exhibits a continuous behavior without any discontinuous jumps, while possessing a non-constant initial value. Evidently, this methodology has proven to yield commendable outcomes, as illustrated in Fig. 6.

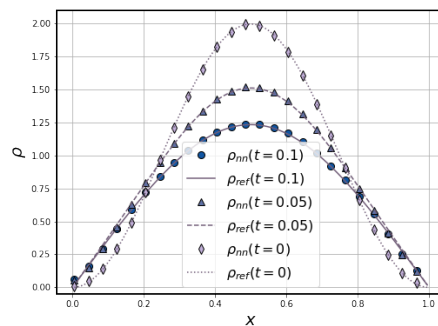


Figure 6: Problem 1—Case II. Plot of density ρ at $t=0.05,0.1$: APNNs (marker) vs. Ref (line). $\varepsilon=10^{-8}$ and the units of neural networks are $[2,128,128,128,128,128,1]$ for ρ and $[3,256,256,256,256,256,1]$ both for r and j . Batch size is 1024 in domain, 512×2 on boundary and 512 on initial condition. $\lambda_3 = \lambda_4 = \lambda_7 = 10$ and others are set to be 1. Relative ℓ^2 error of APNNs is 1.25×10^{-2} .

Case III. Uncertainty quantification problem with inflow condition and ($\varepsilon=10^{-5}$)

Next, we contemplate an uncertainty quantification problem ($\varepsilon=10^{-5}$):

$$\varepsilon \partial_t f + v \partial_x f = \frac{\sigma_S(z)}{\varepsilon} \left(\frac{1}{2} \int_{-1}^1 f dv' - f \right), \quad x_L < x < x_R, \quad -1 \leq v \leq 1, \quad (3.7)$$

with scattering coefficient

$$\sigma_S(\mathbf{z}) = 1 + \frac{1}{10} \sum_{i=1}^{10} \prod_{j=1}^i z^j, \mathbf{z} = (z^1, z^2, \dots, z^{10}) \sim \mathcal{U}([-1, 1]^{10}), \quad (3.8)$$

and in-flow boundary condition $F_L(v) = 1, F_R(v) = 0$, and initial condition $f_0(x, v) = 0$.

In order to address this issue, we incorporate the 10-dimensional stochastic vector \mathbf{z} as a constituent of the input components of the deep neural networks for ρ, r, j . Similarly, it is possible to derive the empirical APNN risk for the even-odd system of linear transport equation with uncertainties in the following manner

$$\mathcal{R}_{\text{APNN, uq}}^\varepsilon = \mathcal{R}_{\text{residual}}^\varepsilon + \mathcal{R}_{\text{constraint}}^\varepsilon + \mathcal{R}_{\text{initial}}^\varepsilon + \mathcal{R}_{\text{boundary}}^\varepsilon, \quad (3.9)$$

where $\mathcal{R}_{\text{residual}}^\varepsilon, \mathcal{R}_{\text{constraint}}^\varepsilon, \mathcal{R}_{\text{initial}}^\varepsilon, \mathcal{R}_{\text{boundary}}^\varepsilon$ are denoted by

$$\begin{aligned} \mathcal{R}_{\text{residual}}^\varepsilon &= \frac{\lambda_1}{N_1^{(1)}} \sum_{i=1}^{N_1^{(1)}} |\varepsilon^2 \partial_t r_\theta^{\text{NN}}(\mathbf{z}_i, t_i, x_i, v_i) + \varepsilon^2 v \partial_x j_\theta^{\text{NN}}(\mathbf{z}_i, t_i, x_i, v_i) \\ &\quad - \sigma_S(\mathbf{z}_i) (\rho_\theta^{\text{NN}}(\mathbf{z}_i, t_i, x_i) - r_\theta^{\text{NN}}(\mathbf{z}_i, t_i, x_i, v_i))|^2 \\ &\quad + \frac{\lambda_2}{N_1^{(2)}} \sum_{i=1}^{N_1^{(2)}} |\varepsilon^2 \partial_t j_\theta^{\text{NN}}(\mathbf{z}_i, t_i, x_i, v_i) + v \partial_x r_\theta^{\text{NN}}(\mathbf{z}_i, t_i, x_i, v_i) - (-\sigma_S(\mathbf{z}_i) j_\theta^{\text{NN}}(\mathbf{z}_i, t_i, x_i, v_i))|^2 \\ &\quad + \frac{\lambda_3}{N_1^{(3)}} \sum_{i=1}^{N_1^{(3)}} |\partial_t \rho_\theta^{\text{NN}}(\mathbf{z}_i, t_i, x_i) + \langle v \partial_x j_\theta^{\text{NN}} \rangle(\mathbf{z}_i, t_i, x_i)|^2, \\ \mathcal{R}_{\text{constraint}}^\varepsilon &= \frac{\lambda_4}{N_2} \sum_{i=1}^{N_2} |\rho_\theta^{\text{NN}}(\mathbf{z}_i, t_i, x_i) - \langle r_\theta^{\text{NN}} \rangle(\mathbf{z}_i, t_i, x_i)|^2, \\ \mathcal{R}_{\text{initial}}^\varepsilon &= \frac{\lambda_5}{N_3} \sum_{i=1}^{N_3} |\rho_\theta^{\text{NN}}(\mathbf{z}_i, 0, x_i) - \langle f_0 \rangle(\mathbf{z}_i, x_i)|^2 + \frac{\lambda_6}{N_4} \sum_{i=1}^{N_4} |\mathcal{I}(r_\theta^{\text{NN}} + \varepsilon j_\theta^{\text{NN}})(\mathbf{z}_i, x_i, v_i) - f_0(\mathbf{z}_i, x_i, v_i)|^2, \\ \mathcal{R}_{\text{boundary}}^\varepsilon &= \frac{\lambda_7}{N_5} \sum_{i=1}^{N_5} |\mathcal{B}(r_\theta^{\text{NN}} + \varepsilon j_\theta^{\text{NN}})(\mathbf{z}_i, t_i, x_i, v_i) - F_B(\mathbf{z}_i, t_i, x_i, v_i)|^2. \end{aligned}$$

Here, $N_1^{(1)}, N_1^{(2)}, N_1^{(3)}, N_2, \dots, N_5$ is the number of sample points of corresponding domain.

To assess the numerical performance, we evaluate the value of ρ at specific time instances, namely $t = 0.05, 0.1$. This evaluation is based on computing the expected outcome over 10^3 simulation iterations, considering \mathbf{z} as a vector comprising elements z^1, z^2, \dots, z^{10} with each z^i generated uniformly from $[-1, 1]$.

Fig. 7 exhibits the anticipated density ρ , trained using APNNs, alongside the reference solutions at time $t = 0.05, 0.1$. The results vividly demonstrate the exceptional capabilities of APNNs when dealing with high-dimensional problems.

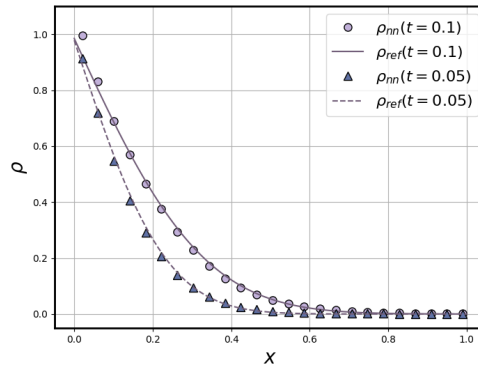


Figure 7: Problem 1—Case III. Plot of density ρ by taking expectation for z at $t=0.05, 0.1$ for APNNs (marker) and Ref (line). $\varepsilon = 10^{-5}$, $\sigma_S(z) = 1 + \frac{1}{10} \sum_{i=1}^{10} \prod_{j=1}^i z^j$ and the units of neural networks are $[22, 64, 128, 256, 256, 128, 64, 1]$ for ρ and $[23, 128, 256, 512, 512, 256, 128, 1]$ for r, j . Batch size is 1024 in domain, 512×2 for boundary condition and 256 for initial condition. $\lambda_5 = \lambda_7 = 10$ and others are set to be 1. Relative ℓ^2 error of APNNs is 3.90×10^{-2} .

3.3 Problem 2: APNNs for solving Boltzmann-BGK equations

Consider the Boltzmann-BGK equation

$$\partial_t f + v \cdot \nabla_x f = \frac{1}{\varepsilon} (M(U) - f), \quad v \in \mathbb{R}. \quad (3.10)$$

and recall the system of BGK model for our APNN is

$$\begin{cases} \varepsilon (\partial_t f + v \partial_x f) = M(U) - f, \\ \partial_t U + \nabla_x \cdot \langle v m f \rangle = 0, \\ U = \langle m f \rangle. \end{cases}$$

Initial local thermodynamics equilibrium is considered for all tests:

$$f(0, x, v) = \frac{\rho_0}{(2\pi T_0)^{\frac{1}{2}}} \exp\left(-\frac{|v - u_0|^2}{2T_0}\right) := f_0(x, v).$$

For these tests, a classical “Riemann-like” problem with Sod like initial data is considered.

$$\begin{aligned} \rho_0(t, x) &= \rho_L, & u_0(t, x) &= u_L, & T_0(t, x) &= T_L, & x &\leq 0, \\ \rho_0(t, x) &= \rho_R, & u_0(t, x) &= u_R, & T_0(t, x) &= T_R, & x &> 0. \end{aligned}$$

By saying “Riemann-like”, we allow the initial data to be a smoothed curve connecting two constants of each macroscopic quantities instead of just two constants (see the following test cases I, II, III, IV, V), i.e.,

$$\begin{aligned} \rho_0(t, x_L) &= \rho_L, & \rho_0(t, x_R) &= \rho_R, \\ u_0(t, x_L) &= u_L, & u_0(t, x_R) &= u_R, \\ T_0(t, x_L) &= T_L, & T_0(t, x_R) &= T_R, \end{aligned}$$

where

$$W_L = (\rho_L, u_L, T_L)^T, W_R = (\rho_R, u_R, T_R)^T.$$

Due to the finite propagation speed, the above conditions hold as long as the waves initially started from the Riemann-like initial data have not reached the computational boundaries in the duration of the computation time.

Numerically, one can construct four DNNs as follows:

$$f_\theta^{\text{NN}}(t, x, v) := \ln \left(1 + \exp(\tilde{f}_\theta^{\text{NN}}(\bar{t}, x, \bar{v})) \right) > 0, \quad (3.11)$$

and

$$\begin{aligned} \rho_\theta^{\text{NN}}(t, x) &:= \rho_L^{\frac{x_R-x}{x_R-x_L}} \cdot \rho_R^{\frac{x-x_L}{x_R-x_L}} \cdot \exp \left((x-x_L)(x_R-x) \cdot \tilde{\rho}_\theta^{\text{NN}}(\bar{t}, x) \right) > 0, \\ u_\theta^{\text{NN}}(t, x) &:= \sqrt{(x-x_L)(x_R-x)} \cdot \tilde{u}_\theta^{\text{NN}}(\bar{t}, x) + \frac{x_R-x}{x_R-x_L} u_L + \frac{x-x_L}{x_R-x_L} u_R, \\ T_\theta^{\text{NN}}(t, x) &:= T_L^{\frac{x_R-x}{x_R-x_L}} \cdot T_R^{\frac{x-x_L}{x_R-x_L}} \cdot \exp \left((x-x_L)(x_R-x) \cdot \tilde{T}_\theta^{\text{NN}}(\bar{t}, x) \right) > 0, \end{aligned} \quad (3.12)$$

which $\rho_\theta^{\text{NN}}, u_\theta^{\text{NN}}, T_\theta^{\text{NN}}$ automatically satisfy the boundary constraint which we find can improve the numerical performance. In this problem, to keep f positive, $\ln(1 + \exp(\cdot))$ is applied for constructing f_θ^{NN} . The advantage of this structure lies in the parity of magnitudes between f_θ^{NN} and $\tilde{f}_\theta^{\text{NN}}$ when their magnitude exceeds a certain threshold.

The APNN empirical risk for the system of Boltzmann-BGK equation is

$$\mathcal{R}_{\text{APNN, BGK}}^\varepsilon = \mathcal{R}_{\text{residual}}^\varepsilon + \mathcal{R}_{\text{claw}}^\varepsilon + \mathcal{R}_{\text{constraint}}^\varepsilon + \mathcal{R}_{\text{boundary}}^\varepsilon + \mathcal{R}_{\text{initial}}^\varepsilon, \quad (3.13)$$

where $\mathcal{R}_{\text{residual}}^\varepsilon, \mathcal{R}_{\text{claw}}^\varepsilon, \mathcal{R}_{\text{constraint}}^\varepsilon, \mathcal{R}_{\text{boundary}}^\varepsilon, \mathcal{R}_{\text{initial}}^\varepsilon$ are denoted by

$$\begin{aligned} \mathcal{R}_{\text{residual}}^\varepsilon &= \frac{\lambda_1}{N_1} \sum_{i=1}^{N_1} |\varepsilon(\partial_t f_\theta^{\text{NN}}(t_i, x_i, v_i) + v_i \nabla_x f_\theta^{\text{NN}}(t_i, x_i, v_i)) - (M(U_\theta^{\text{NN}}) - f_\theta^{\text{NN}})(t_i, x_i, v_i)|^2, \\ \mathcal{R}_{\text{claw}}^\varepsilon &= \frac{\lambda_2}{N_2} \sum_{i=1}^{N_2} |\partial_t U_\theta^{\text{NN}}(t_i, x_i) + \nabla_x \langle v m f_\theta^{\text{NN}} \rangle(t_i, x_i)|^2, \\ \mathcal{R}_{\text{constraint}}^\varepsilon &= \frac{\lambda_3}{N_3} \sum_{i=1}^{N_3} |U_\theta^{\text{NN}}(t_i, x_i) - \langle m f_\theta^{\text{NN}} \rangle(t_i, x_i)|^2, \\ \mathcal{R}_{\text{boundary}}^\varepsilon &= \frac{\lambda_4}{N_4} \sum_{i=1}^{N_4} |W_\theta^{\text{NN}}(t_i, x_L) - W_L|^2 + |W_\theta^{\text{NN}}(t_i, x_R) - W_R|^2, \\ \mathcal{R}_{\text{initial}}^\varepsilon &= \frac{\lambda_5}{N_5} \sum_{i=1}^{N_5} |W_\theta^{\text{NN}}(0, x_i) - W_0(x_i)|^2 + \frac{\lambda_6}{N_6} \sum_{i=1}^{N_6} |f_\theta^{\text{NN}}(0, x_i, v_i) - f_0(x_i, v_i)|^2. \end{aligned} \quad (3.14)$$

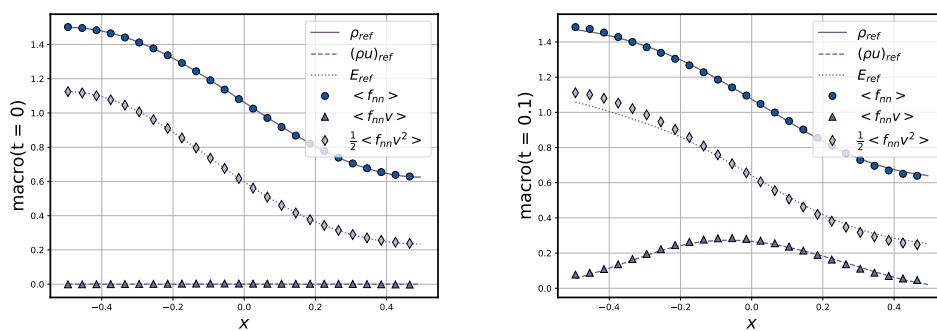
Here, $N_i (i=1, \dots, 6)$ is the number of sample points of corresponding domain.

These cases are studied in Problem 2.

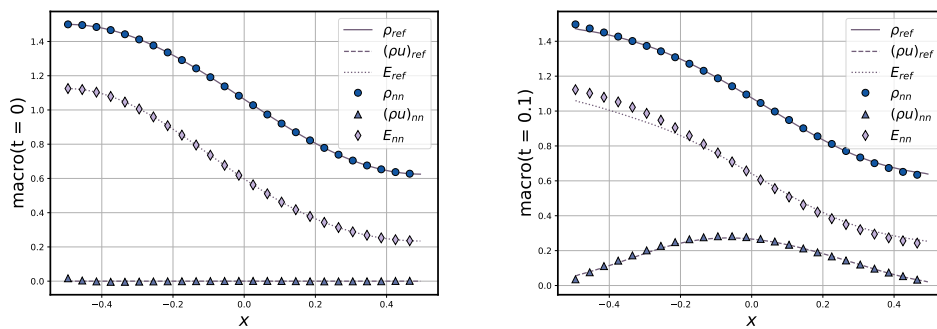
Case I: $\varepsilon = 10^{-3}$

$$\begin{aligned}\rho_0(x) &= 1.5 + (0.625 - 1.5) \cdot \frac{\sin(\pi x) + 1}{2}, \\ u_0(x) &= 0, \\ T_0(x) &= 1.5 + (0.75 - 1.5) \cdot \frac{\sin(\pi x) + 1}{2}.\end{aligned}$$

Fig. 8 illustrates the graph representing approximate macroscopic properties at time $t = 0, 0.1$. It is evident that the approximate density, momentum, and energy exhibit superior performance compared to those derived from the approximate function f .



(a) The integrals of approximate f_{nn} vs. reference solutions. *Left: $t=0$ and Right: $t=0.1$.*



(b) The approximate $\rho_{nn}, u_{nn}, T_{nn}$ vs. reference solutions. *Left: $t=0$ and Right: $t=0.1$.*

Figure 8: Problem 2—Case I. Plot of density, momentum and energy at time $t = 0, 0.1$: Approximated by APNNs (marker) vs. Ref (line). $\varepsilon = 10^{-3}$ and the units of neural networks are $[3, 128, 128, 128, 128, 128, 1]$ for f and $[2, 64, 64, 64, 64, 64, 1]$ both for ρ, u and T . Batch size is 512 in domain, and 256 on initial condition. $\lambda_5 = (1, 10, 10), \lambda_6 = 10$ and others are set to be 1. For $t = 0$: mean square error of density, momentum and energy are $7.16e-8, 4.50e-6, 8.13e-7$. For $t = 0.1$: relative l^2 error of density, momentum and energy are $5.43e-3, 6.35e-3, 4.47e-2$.

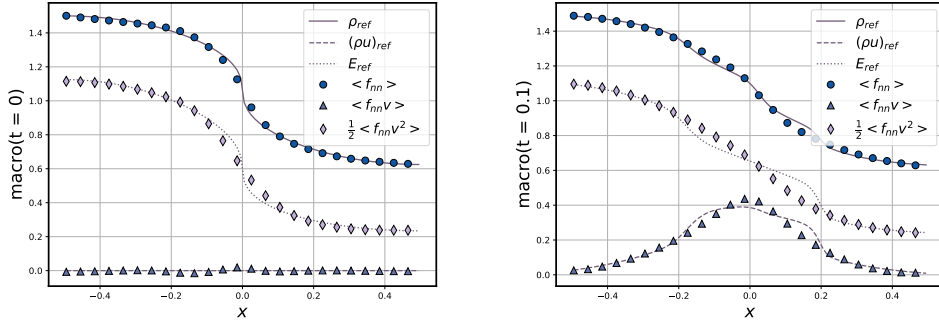
Case II: $\varepsilon = 10^{-3}$

$$\rho_0(x) = 1.5 + (0.625 - 1.5) \cdot \frac{\sin^3(\pi x) + 1}{2},$$

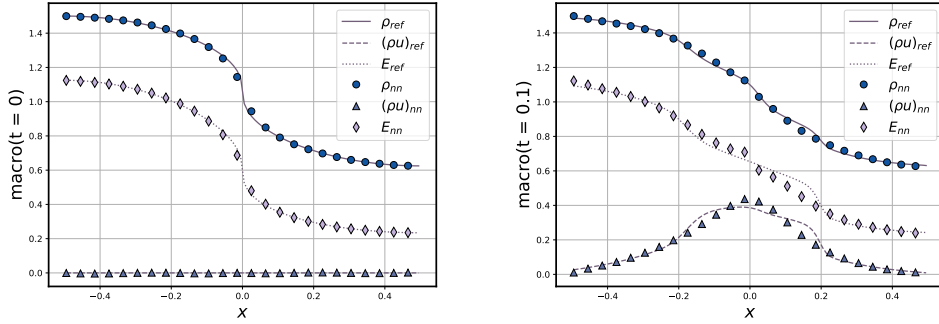
$$u_0(x) = 0,$$

$$T_0(x) = 1.5 + (0.75 - 1.5) \cdot \frac{\sin^3(\pi x) + 1}{2}.$$

Fig. 9 illustrates the plot depicting the approximated macroscopic quantities at $t = 0, 0.1$. It is noteworthy that the steep slope of $\rho(0, x)$ and $T(0, x)$ at $x = 0$ poses a considerable challenge for obtaining accurate solutions through approximation. The key observation in this scenario is that approximating the moments of f , namely, ρ, u, T , is comparatively simpler than approximating f itself. This assertion holds true across all the test cases.



(a) The integrals of approximate f_{nn} vs. reference solutions. *Left: $t = 0$ and Right: $t = 0.1$.*



(b) The approximate $\rho_{nn}, u_{nn}, T_{nn}$ vs. reference solutions. *Left: $t = 0$ and Right: $t = 0.1$.*

Figure 9: Problem 2—Case II. Plot of density, momentum and energy at time $t = 0, 0.1$: Approximated by APNNs (marker) vs. Ref (line). $\varepsilon = 10^{-3}$ and the units of neural networks are $[3, 128, 128, 128, 128, 128, 128, 1]$ for f and $[2, 64, 64, 64, 64, 64, 64, 1]$ both for ρ, u and T . Batch size is 512 in domain, and 256 on initial condition. $\lambda_5 = (1, 10, 10)$ and others are set to be 1. For $t = 0$: mean square error of density, momentum and energy are $1.29e-4, 6.34e-6, 4.41e-5$. For $t = 0.1$: relative l^2 error of density, momentum and energy are $1.36e-2, 2.00e-2, 3.99e-2$.

Case III: $\varepsilon = 10^{-3}$

$$\begin{aligned}\rho_0(x) &= 1.5 + (0.625 - 1.5) \cdot \frac{\tanh(10x) + 1}{2}, \\ u_0(x) &= 0, \\ T_0(x) &= 1.5 + (0.75 - 1.5) \cdot \frac{\tanh(10x) + 1}{2}.\end{aligned}$$

Fig. 10 depicts the graph illustrating the plot of approximate macroscopic quantities at $t=0,0.1$. In this particular scenario, the gradient of $\rho(0,x)$ and $T(0,x)$ at $x=0$ exhibits a seamless behavior. It is evident that the approximate solutions align well with the reference solutions; however, the first moment computed by the approximate function f yields unsatisfactory outcomes in the vicinity of $x=0$. This observation concurs with the findings presented in cases I and II.

Case IV: $\varepsilon = 1$

$$\begin{aligned}\rho_0(x) &= 1.5 + (0.625 - 1.5) \cdot \frac{\tanh(20x) + 1}{2}, \\ u_0(x) &= 0, \\ T_0(x) &= 1.5 + (0.75 - 1.5) \cdot \frac{\tanh(20x) + 1}{2}.\end{aligned}$$

The plot displayed in Fig. 11 illustrates the representation of estimated macroscopic quantities at time instances $t=0,0.1$. It is worth noting that this particular scenario closely resembles a realistic problem. In this context, our proposed APNN method demonstrates commendable efficacy by offering favorable solutions when compared to the reference solutions.

Fig. 12 illustrates the relative l^2 discrepancy in density, momentum, and energy throughout the training process. An intriguing observation emerges, wherein the convergence of density and momentum outpaces that of energy across all instances, encompassing $\varepsilon = 1$ and 10^{-3} . Training the energy component proves notably more challenging.

Table 1 documents the mean square error of risks $\mathcal{R}_{\text{residual}}^\varepsilon, \mathcal{R}_{\text{claw}}^\varepsilon$, and $\mathcal{R}_{\text{constraint}}^\varepsilon$ across these scenarios.

Table 1: Mean square errors of risks $\mathcal{R}_{\text{residual}}^\varepsilon, \mathcal{R}_{\text{claw}}^\varepsilon$ and $\mathcal{R}_{\text{constraint}}^\varepsilon$ in terms of four cases.

Case	Risk	$\mathcal{R}_{\text{residual}}^\varepsilon$		$\mathcal{R}_{\text{claw}}^\varepsilon$		$\mathcal{R}_{\text{constraint}}^\varepsilon$		
		density	momentum	energy	0-order	1-order	2-order	
I		3.92e-6	7.01e-7	1.70e-5	6.42e-7	1.80e-6	1.77e-5	8.17e-7
II		1.30e-5	1.16e-5	1.97e-5	9.58e-6	1.67e-5	4.20e-5	1.63e-5
III		1.54e-5	1.81e-6	4.67e-6	3.73e-6	1.95e-6	1.61e-5	8.20e-7
IV		6.24e-5	5.90e-6	1.30e-5	2.09e-5	3.62e-6	6.08e-6	5.07e-6

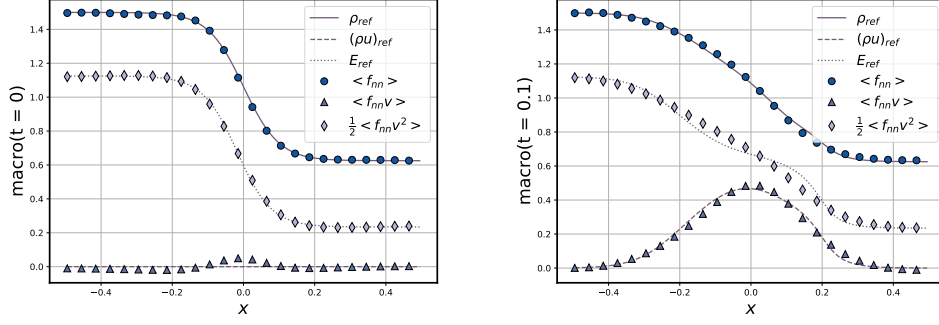
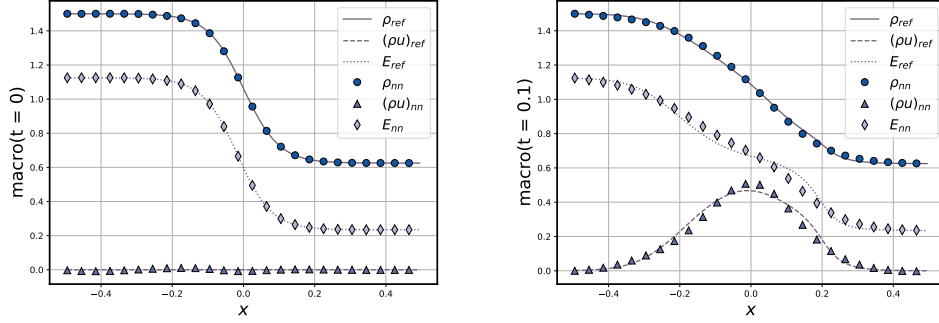
(a) The integrals of approximate f_{nn} vs. reference solutions. *Left: $t=0$ and Right: $t=0.1$.*(b) The approximate $\rho_{nn}, u_{nn}, T_{nn}$ vs. reference solutions. *Left: $t=0$ and Right: $t=0.1$.*

Figure 10: Problem 2—Case III. Plot of density, momentum and energy at time $t=0,0.1$: Approximated by APNNs (marker) vs. Ref (line). $\varepsilon=10^{-3}$ and the units of neural networks are $[3,128,128,128,128,128,128,1]$ for f and $[2,64,64,64,64,64,64,1]$ both for ρ, u and T . Batch size is 512 in domain, and 256 on initial condition. $\lambda_5 = (1,10,10), \lambda_6 = 10$ and others are set to be 1. For $t=0$: mean square error of density, momentum and energy are $4.87e-8, 1.22e-6, 3.29e-8$. For $t=0.1$: relative l^2 error of density, momentum and energy are $6.19e-3, 1.78e-2, 3.60e-2$.

Case V: $\varepsilon = 10^{-2}$

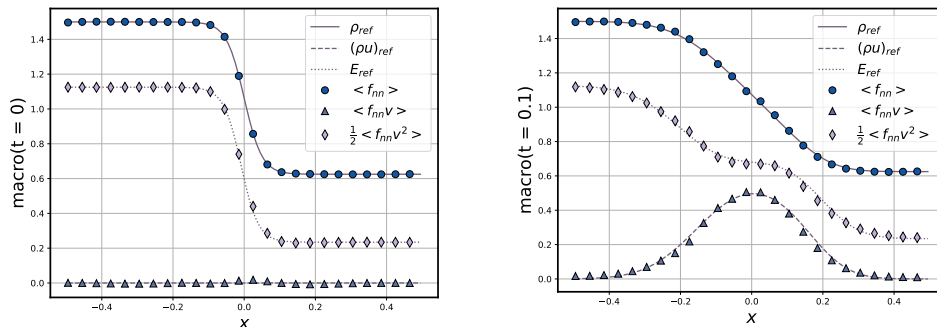
$$\rho_0(x) = \begin{cases} 1.5, & x < 0, \\ 0.625x \geq 0, \end{cases}$$

$$u_0(x) = 0,$$

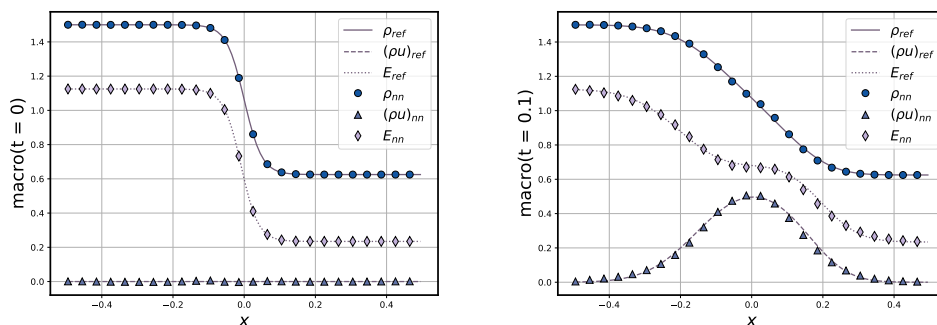
$$T_0(x) = \begin{cases} 1.5, & x < 0, \\ 0.75x \geq 0. \end{cases}$$

The figure depicted in Fig. 13 illustrates the graphical representation of the estimated macroscopic variables at the instant of $t=0$.

Fig. 14 depicts the graphical representation of the approximated macroscopic quantities spanning from $t=0.005$ to $t=0.05$. Notably, at $t=0.005 < \varepsilon$, a discernible transition in the macroscopic solutions becomes evident.



(a) The integrals of approximate f_{nn} vs. reference solutions. *Left: $t=0$ and Right: $t=0.1$.*



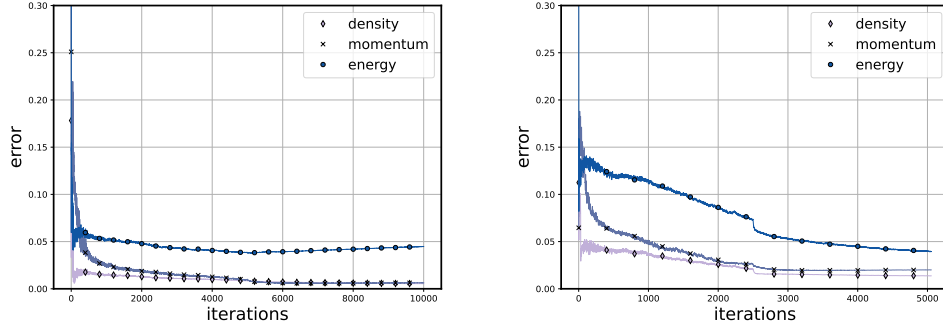
(b) The approximate $\rho_{nn}, u_{nn}, T_{nn}$ vs. reference solutions. *Left: $t=0$ and Right: $t=0.1$.*

Figure 11: Problem 2—Case IV. Plot of density, momentum and energy at time $t=0,0.1$: Approximated by APNNs (marker) vs. Ref (line). $\varepsilon=1$ and the units of neural networks are $[3,128,128,128,128,128,1]$ for f and $[2,64,64,64,64,64,1]$ both for ρ, u and T . Batch size is 512 in domain, and 256 on initial condition. $\lambda_5 = (1,10,10), \lambda_6 = 10$ and others are set to be 1. For $t=0$: mean square error of density, momentum and energy are $9.89e-8, 2.34e-6, 2.08e-7$. For $t=0.1$: relative l^2 error of density, momentum and energy are $6.41e-3, 8.72e-3, 1.62e-2$.

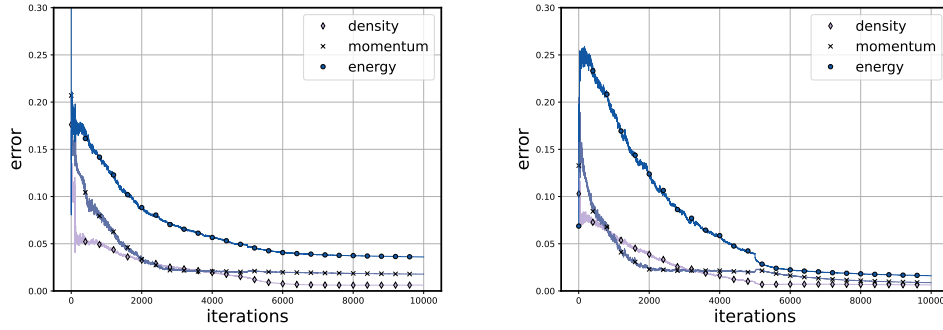
4 Discussion and conclusion

In this paper, we have devised novel and efficient Asymptotic-Preserving Neural Networks (APNNs) to numerically approximate the multiscale kinetic equations involving possibly small Knudsen number. For the linear transport equation with diffusive scaling, our APNN, utilize parity equations, by designing the loss function that captures physical conservation property, and also the inflow boundary condition. For the BGK equation, with the a collision term that exhibits both nonlinearity and non-locality, along with a boundary layer effect, we have devised an APNN method that with a loss that not only follows the equation but also the dynamics of the conserved moments, in addition to precisely enforces the boundary conditions.

During the training process, a phenomenon becomes apparent: the convergence of



(a) *Left*: Case I with $\varepsilon = 10^{-3}$ and *Right*: Case II with $\varepsilon = 10^{-3}$.



(b) *Left*: Case III with $\varepsilon = 10^{-3}$ and *Right*: Case IV with $\varepsilon = 1$.

Figure 12: Problem 2. Plot of the change of error for density, momentum and energy approximated by APNNs.

momentum and energy is slower in comparison to that of density. This discrepancy is likely influenced by the value of ε . The question that arises is how to explain this phenomenon, which needs further study.

Due to the nonlinearity, high dimensionality and multiscale nature of kinetic equations, the construction of the neural network holds tremendous tremendous. Our studies are preliminary but call for more investigations to more physical equations such as the Boltzmann and Landau equations.

Acknowledgement

This work is partially supported by the National Key R&D Program of China Project No. 2020YFA0712000 and Shanghai Municipal of Science and Technology Major Project No. 2021SHZDZX0102. Shi Jin is also supported by NSFC grant No. 11871297. Zheng Ma is also supported by NSFC Grant No. 12031013, No.92270120 and partially supported by Institute of Modern Analysis—A Shanghai Frontier Research Center.

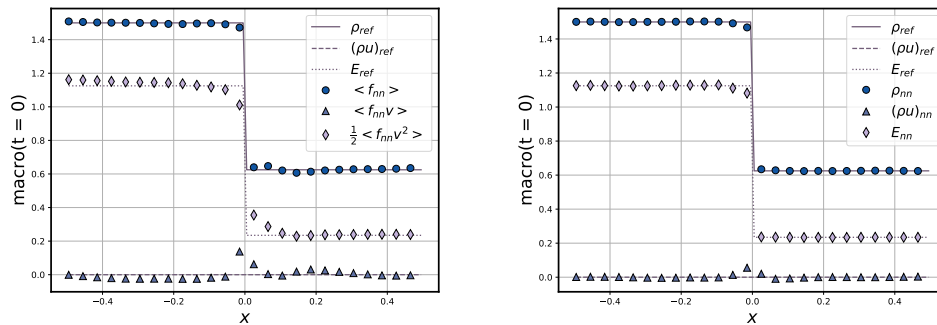


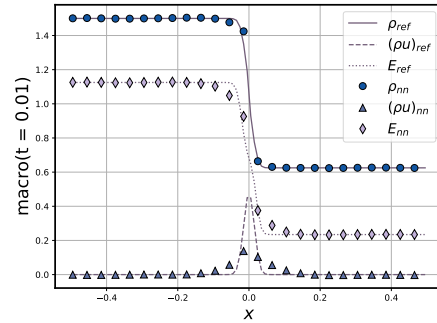
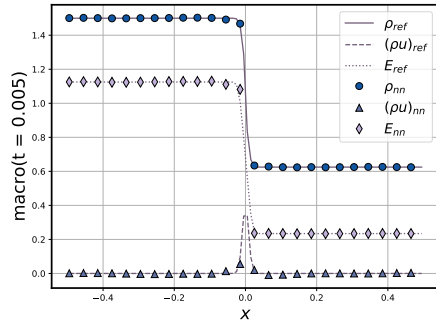
Figure 13: Problem 2—Case V. Plot of density, momentum and energy at time $t=0$: Approximated by APNNs (marker) vs. Ref (line). $\varepsilon=10^{-2}$ and the units of neural networks are $[3,128,128,128,128,128,128,1]$ for f and $[2,96,96,96,96,96,96,1]$ both for ρ, u and T . Batch size is 512 in domain, and 512 on initial condition. $\lambda_3 = (10,10,1), \lambda_5 = (1,100,100), \lambda_6 = 100$ and others are set to be 1.

References

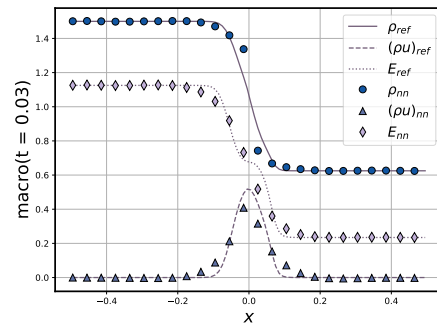
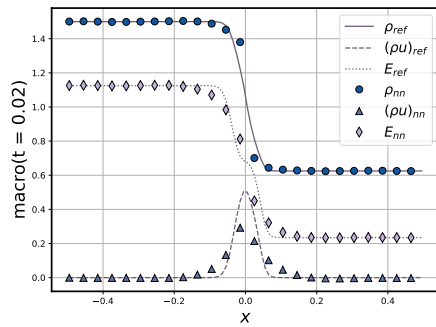
- [1] François Bouchut, François Golse, and Mario Pulvirenti. Kinetic equations and asymptotic theory. Elsevier, 2000.
- [2] Giacomo Dimarco and Lorenzo Pareschi, Numerical methods for kinetic equations. Acta Numerica, 23:369-520, 2014.
- [3] Shi Jin. Asymptotic preserving (AP) schemes for multiscale kinetic and hyperbolic equations: a review. Lecture notes for summer school on methods and models of kinetic theory (M&MKT), Porto Ercole (Grosseto, Italy), pages 177-216, 2010.
- [4] Weinan E. Principles of multiscale modeling. Cambridge University Press, 2011.
- [5] Christian Beck, Martin Hutzenthaler, Arnulf Jentzen, and Benno Kuckuck. An overview on deep learning-based approximation methods for partial differential equations, arXiv preprint arXiv:2012.12348, 2020.
- [6] Zhiqiang Cai, Jingshuang Chen, and Min Liu. Least-squares relu neural network (lsnn) method for linear advection-reaction equation. Journal of Computational Physics, page 110514, 2021.
- [7] Weinan E and Bing Yu. The deep ritz method: A deep learning-based numerical algorithm for solving variational problems. Communications in Mathematics and Statistics, 6(1):1–12, 2018.
- [8] Yulei Liao and Pingbing Ming. Deep nitsche method: Deep ritz method with essential boundary conditions. Communications in Computational Physics, 29(5):1365–1384, 2021.
- [9] Liyao Lyu, Zhen Zhang, Minxin Chen, and Jingrun Chen. Mim: A deep mixed residual method for solving high-order partial differential equations. Journal of Computational Physics, 452:110930, 2022.
- [10] Maziar Raissi, Paris Perdikaris and George E Karniadakis. Physics-informed neural networks: A deep learning framework for solving forward and inverse problems involving nonlinear partial differential equations. Journal of Computational Physics, 378:686–707, 2019.
- [11] Justin Sirignano and Konstantinos Spiliopoulos. DGM: A deep learning algorithm for solving partial differential equations. Journal of Computational Physics, 375:1339–1364, 2018.
- [12] Yaohua Zang, Gang Bao, Xiaojing Ye, and Haomin Zhou. Weak adversarial networks for

- high-dimensional partial differential equations. *Journal of Computational Physics*, page 109409, 2020.
- [13] Zongyi Li, Nikola Borislavov Kovachki, Kamyar Azizzadenesheli, Burigede liu, Kaushik Bhattacharya, Andrew Stuart, and Anima Anandkumar. Fourier neural operator for parametric partial differential equations. In *International Conference on Learning Representations*, 2021.
- [14] Lu Lu, Pengzhan Jin, Guofei Pang, Zhongqiang Zhang, and George Em Karniadakis. Learning nonlinear operators via deeponet based on the universal approximation theorem of operators. *Nature Machine Intelligence*, 3(3):218–229, 2021.
- [15] Lulu Zhang, Tao Luo, Yaoyu Zhang, Weinan E, Zhi-Qin John, and Zheng Ma. Mod-net: A machine learning approach via model-operator-data network for solving pdes. *Communications in Computational Physics*, 32(2):299–335, 2022.
- [16] Zongyi Li, Hongkai Zheng, Nikola Kovachki, David Jin, Haoxuan Chen, Burigede Liu, Kamyar Azizzadenesheli, and Anima Anandkumar. Physics-informed neural operator for learning partial differential equations. *arXiv preprint arXiv:2111.03794*, 2021.
- [17] Sifan Wang, Hanwen Wang, and Paris Perdikaris. Learning the solution operator of parametric partial differential equations with physics-informed deeponets. *Science advances*, 7(40):eabi8605, 2021.
- [18] Wei Xiong, Xiaomeng Huang, Ziyang Zhang, Ruixuan Deng, Pei Sun, and Yang Tian. Koopman neural operator as a mesh-free solver of non-linear partial differential equations. *arXiv preprint arXiv:2301.10022*, 2023.
- [19] Zheng Chen, Liu Liu, and Lin Mu. Solving the linear transport equation by a deep neural network approach. *Discrete and Continuous Dynamical Systems - S*, 15(4):669–686, 2022.
- [20] Hyung Ju Hwang, Jin Woo Jang, Hyeontae Jo, and Jae Yong Lee. Trend to equilibrium for the kinetic fokker-planck equation via the neural network approach. *Journal of Computational Physics*, 419:109665, 2020.
- [21] Shi Jin, Zheng Ma, and Keke Wu. Asymptotic-preserving neural networks for multiscale time-dependent linear transport equations. *Journal of Scientific Computing*, 94(3):57, 2023.
- [22] Shi Jin. Asymptotic-preserving schemes for multiscale physical problems. *Acta Numerica*, 31:415–489, 2022.
- [23] Yulong Lu, Li Wang, and Wuzhe Xu. Solving multiscale steady radiative transfer equation using neural networks with uniform stability. *Research in the Mathematical Sciences*, 9(3):1–29, 2022.
- [24] Hongyan Li, Song Jiang, Wenjun Sun, Liwei Xu, and Guanyu Zhou. A model-data asymptotic-preserving neural network method based on micro-macro decomposition for gray radiative transfer equations. *arXiv preprint arXiv:2212.05523*, 2022.
- [25] Giulia Bertaglia. Asymptotic-preserving neural networks for hyperbolic systems with diffusive scaling. In *Advances in Numerical Methods for Hyperbolic Balance Laws and Related Problems*, pages 23–48. Springer Nature Switzerland, 2023.
- [26] Giulia Bertaglia, Chuan Lu, Lorenzo Pareschi, and Xueyu Zhu. Asymptotic-preserving neural networks for multiscale hyperbolic models of epidemic spread. *Mathematical Models and Methods in Applied Sciences*, 32(10):1949–1985, 2022.
- [27] Qin Lou, Xuhui Meng, and George Em Karniadakis. Physics-informed neural networks for solving forward and inverse flow problems via the boltzmann-bgk formulation. *Journal of Computational Physics*, 447:110676, 2021.
- [28] Kaiming He, Xiangyu Zhang, Shaoqing Ren, and Jian Sun. Deep residual learning for image recognition. In *Proceedings of the IEEE conference on computer vision and pattern recognition*, pages 770–778, 2016.
- [29] Shi Jin, L Pareschi and G Toscani. Uniformly Accurate Diffusive Relaxation Schemes for

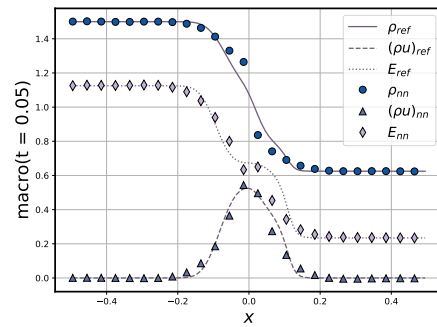
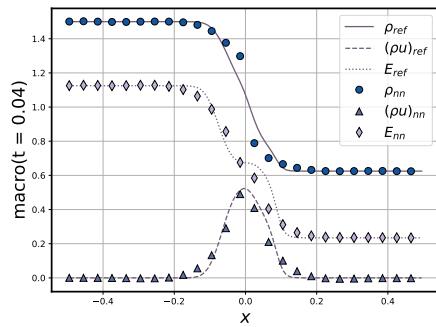
- Multiscale Transport Equations, *SIAM J. Num. Anal.* 38:913-936, 2000.
- [30] Carlo Cercignani. Rarefied gas dynamics: from basic concepts to actual calculations, volume 21. Cambridge university press, 2000.
 - [31] Maurice N Kogan. Rarefied gas dynamics. Springer, 2013.
 - [32] Mounir Bennoune, Mohammed Lemou, and Luc Mieussens. Uniformly stable numerical schemes for the boltzmann equation preserving the compressible navier–stokes asymptotics. *Journal of Computational Physics*, 227(8):3781–3803, 2008
 - [33] Mohammed Lemou and Luc Mieussens. A new asymptotic preserving scheme based on micro-macro formulation for linear kinetic equations in the diffusion limit. *SIAM Journal on Scientific Computing*, 31(1):334–368, 2008.
 - [34] Shi Jin and Zhouping Xin. The relaxation schemes for systems of conservation laws in arbitrary space dimensions. *Communications on pure and applied mathematics*, 48(3):235–276, 1995.
 - [35] Francois Coron and Benoit Perthame. Numerical passage from kinetic to fluid equations. *SIAM Journal on Numerical Analysis*, 28(1):26–42, 1991.
 - [36] F Filber and Shi Jin. A class of asymptotic-preserving schemes for kinetic equations and related problems with stiff sources. *Journal of Computational Physics*, 229(20):7625–7648, 2010.
 - [37] P Bhatnagar, E Gross, and Max Krook. A model for collision processes in gases. *Physical Review*, 94(3):511, 1954.
 - [38] Shi Jin and Bokai Yan. A class of asymptotic-preserving schemes for the Fokker-Planck-Landau equation. *Journal of Computational Physics*, 230(17):6420-6437, 2011.
 - [39] Irene M.Gamba, Shi Jin and Liu Liu. Micro-macro decomposition based asymptotic-preserving numerical schemes and numerical moments conservation for collisional non-linear kinetic equations. *Journal of Computational Physics*, 382:264-290, 2019.
 - [40] Kun Xu. A gas-kinetic bgk scheme for the navier–stokes equations and its connection with artificial dissipation and godunov method. *Journal of Computational Physics*, 171(1):289–335, 2001.
 - [41] Hua-Zhong Tang. Gas-kinetic schemes for compressible flow of real gases. *Computers & Mathematics with Applications*, 41(5-6):723–734, 2001.
 - [42] Diederik P Kingma and Jimmy Ba. Adam: A method for stochastic optimization. In *ICLR*, 2015.
 - [43] Lu Lu, Xuhui Meng, Zhiping Mao, and George Em Karniadakis. Deepxde: A deep learning library for solving differential equations. *SIAM Review*, 63(1):208–228, 2021.



(a) The approximate $\rho_{nn}, u_{nn}, T_{nn}$ vs. reference solutions. *Left: $t = 0.005$ and Right: $t = 0.01$.*



(b) The approximate $\rho_{nn}, u_{nn}, T_{nn}$ vs. reference solutions. *Left: $t = 0.02$ and Right: $t = 0.03$.*



(c) The approximate $\rho_{nn}, u_{nn}, T_{nn}$ vs. reference solutions. *Left: $t = 0.04$ and Right: $t = 0.05$.*

Figure 14: Plot of density, momentum and energy at time $t = 0.005$ to 0.05 : Approximated by APNNs (marker) vs. Ref (line).